

# Antenna system characteristic and solar radio burst observation

Sha Li<sup>1,2,3</sup>, Yi-hua Yan<sup>1,2</sup>, Zhi-jun Chen<sup>1,2</sup>, Wei Wang<sup>1,2</sup> and Dong-hao Liu<sup>1</sup>

<sup>1</sup> Key Laboratory of Solar Activity, National Astronomical Observatories, Chinese Academy of Sciences; Datun Road 20A, Chaoyang District, Beijing 100012, China *lisha1400@bao.ac.cn*

<sup>2</sup> Key Laboratory of Radio Astronomy, Chinese Academy of Science

<sup>3</sup> University of Chinese Academy of Sciences 10049

**Abstract** Chinese Spectral Radio Heliograph (CSRH) is an advanced aperture synthesis solar radio heliograph, developed by National Astronomical Observatories, Chinese Academy of Sciences independently. It consists of 100 reflector antennas, which are grouped into two antenna arrays (CSRH-I and CSRH-II) for low and high frequency bands respectively. The frequency band of CSRH-I is 0.4-2GHz and for CSRH-II, the frequency band is 2-15GHz. In the antenna and feed system, CSRH uses an Eleven feed to receive signals coming from the Sun, the radiation pattern with lower side lobe and back lobe of the feed is well radiated. The characteristics of gain  $G$  and antenna noise temperature  $T$  effect the quality of solar radio imaging. For CSRH, measured  $G$  is larger than 60 dBi and  $T$  is less than 120K, after CSRH-I was established, we have successfully captured a solar radio burst between 1.2-1.6GHz on November 12, 2010 through this instrument and this event was confirmed through the observation of Solar Broadband Radio Spectrometer (SBRS) at 2.84GHz and Geostationary Operational Environmental Satellite (GOES). In addition, an image obtained from CSRH-I clearly reveals the profile of the solar radio burst. The other observational work is the imaging of Fengyun-2E geosynchronous satellite which is assumed to be a point source. This data processing method indicates that, the method of deleting errors about dirty image could be used for processing other surface sources.

**Key words:** Reflector antenna :Noise Temperature : Eleven antenna : Low cross polarization : Aperture synthesis

## 1 INTRODUCTION

In solar radio observations, the Sun exhibits a variety of large dynamic phenomena in different

phenomena reveal the links between solar astronomy and other branches of physics. For example, magnetohydrodynamics(MHD)and plasma physics can be well explained through solar observations. The fundamental concept behind MHD shows that the magnetic fields can induce currents in a moving conductive fluid, which creates forces on the fluid and also changes the magnetic field itself. The plasma is composed of ions and electrons, it is the key to understand the propagation of radio wave coming from the Sun. CSRH observations with high spatial resolution could provide important diagnosing tools on the magnetic field, solar radio density, plasma temperature,etc (Yan 2008). Imaging spectroscopy over centimeter and decimeter wavelength range are important for CSRH to explain fundamental problems such as energy release, particle acceleration and particle transport.

In view of the available solar radio astronomical instruments all over the world, two main kinds of instruments are used in solar observations. One is radio heliograph at single or discrete frequencies, for example, Nancay Radio Heliograph (NRH) observes the Sun at 150, 164, 237, 327 and 410MHz, Nobeyama Radio Heliograph (NoRH) (Nakajima 1994) observes the Sun at 17 and 34GHz and Siberian Solar Radio Telescope(SSRT)(Uralov 1998) observes the Sun at 5.7GHz (Les 2014). The other instruments are spectrometers at certain frequency band and frequency points, such as Solar Broadband Radio Spectrometer (SBRS) at 1-2GHz, 2.6-3.8GHz, 5.2-7.6GHz, 2.84GHz. Although scientists have developed some good theoretic models from the observations of these instruments, there were still a lot of phenomena that could not be explained by the current observations and theories. So a radio heliograph which could give solar images in ultra wide band width is required. Now, an undergoing CSRH with high temporal, high spatial and high spectral resolution will create radio images in ultra wide band width. It could be expected to provide better observations explaining these phenomena(Chen 2014).

The aim of CSRH is to provide a new tool observing solar radio emissions, including radio bursts from primary energy release sites of the solar energetic events such as flares and coronal mass ejections (CMEs). Solar radio bursts are rich with different types during solar flares, which are believed due to the sudden energy release process of the solar magnetic field topological reorganization or through the magnetic reconnection. CSRH will make full disk of solar radio images with multiple frequency channels with 25ms cadence in the measurement.

Errors in radio heliograph, such as correlation-based error, antenna pointing precision error, the receiver output noise error. Because of so many errors, we have to calibrate the phase and amplitude errors of each output signal. The amplitude calibration is performed by comparing and equalizing the signal levels in the element of antenna array. With consideration of the instrument's errors, the measurement of phase calibration between different channels is to make use of celestial radio source from this theory, and the phase corrections are applied to the actual solar observations. As we know, the sensitivity of a point source is proportional to the effective collecting area of the telescope, this area is decided by one antenna multiplied by the number of the antennas, in fact, the Sun is larger than the beam of the individual antennas (Liu 2007), so a number of pointing

To evaluate CSRH antenna system, the gain and noise temperature of the antenna, the sensitivity of the receiver should be measured. This paper presents a method for computing the characteristics of CSRH, and provides the results of the antenna gain  $G$  and antenna temperature  $T$ . This paper also gives two observation work, one is solar radio burst observation and the other is satellite source imaging. The solar radio burst was observed by CSRH-I 5-element array on December 12, 2010. This instance was also captured by SBRS at 2.84GHz and GOES in X-ray. Another result came from observing the Fengyun-2E geosynchronous satellite at the height of nearly 35600km. The output signal from each antenna was calibrated with reference to the known standard satellite source. Then, we produced the images by using Common Astronomy Software Application (CASA) which is an image layout software used for aperture synthesis telescope.

The content of this paper is arranged as follows. Section II gives the description of CSRH along with the measured and simulated radiation patterns. In section III, the antenna noise temperature and gain of the system are calculated in detail. Section IV gives images of the solar radio burst and satellite point source, which are drew by using the calibrated data of CSRH. Finally, the conclusions are given in section V.

## 2 ANTENNA SYSTEM

### 2.1 About CSRH

CSRH is a radio interferometer which contains 100 parabolic reflector antennas. CSRH-I consists of 40 4.5-m-diameter antennas operating between 0.4-2GHz, CSRH-II consists of 60 2-m-diameter antennas from 2 to 15GHz. (Figure 1) shows the photo of constructed CSRH, which includes 3.87 hectares and locates in Inner Mongolia, 400km away from Beijing. The exact geographical coordinates of the central antenna is located at 115 degrees 15 minutes 1.8 seconds east longitude and 42 degrees 12 minutes 42.6 seconds north latitude. The antenna configuration (Yan 2008) is a non-redundant array with good  $(u,v)$  coverage. The baseline vector has components  $(u,v,w)$ , where  $w$  points in the direction of interest.  $u,v,w$  are measured in wavelengths at center frequency of the RF signal band, and in the directions towards the East, the North, and the phase tracking center respectively. For  $(u,v)$  coverage, if we assume the spatial frequencies as follows:

$$\vec{f} = (u, v) \quad (1)$$

which are the conjugated coordinates of the spatial coordinates  $(x,y)$  in the image plane. While  $(x,y)$  measure angles, usually expressed in arcseconds, spatial frequencies measure distance in the incident wavefront measured in wavelength units, they are usually expressed in  $arcsec^{-1}$ , shown in (Equation 2),

$$\vec{f} = (u, v) = \frac{1}{\lambda} (\Delta X, \Delta Y) \quad (2)$$

During the imaging process, the incoming wavefront is spatially sampled by the radio heliograph, we need to make our measurements in a plane and measured in terms of the wavelength.



**Fig. 1** A view of CSRH

depends on the array configuration. The Fourier components of the object are measured at different spatial frequencies. (Figure 2) shows the arrangement of CSRH-I. (Figure 3) gives the  $(u,v)$  coverage (Lindsay 2008) of (Figure 2). All the antennas are arranged in three spiral arms (named A axis, B axis and C axis) respectively.

For multiple-element antenna arrays, it is convenient to specify the antenna positions relative to the reference point measured in a Cartesian coordinate system, a system with axes pointing towards hour-angle  $h$  and declination  $\delta$  equal to  $(h=0, \delta = 0)$  for X,  $(h=-6^h, \delta = 0)$  for Y, and  $(\delta = 90 \text{ deg})$  for Z. If we assume  $L_X$ ,  $L_Y$  and  $L_Z$  are the corresponding coordinate differences for two antennas, the baseline components  $(u,v,w)$  are given by (Equation 3):

$$\begin{pmatrix} u \\ v \\ w \end{pmatrix} = \frac{1}{\lambda} \begin{pmatrix} \sin H_0 & \sin H_0 & 0 \\ -\sin \delta_0 \cos H_0 & \sin \delta_0 \sin H_0 & \cos \delta_0 \\ \cos \delta_0 \cos H_0 & -\cos \delta_0 \sin H_0 & \sin \delta_0 \end{pmatrix} \begin{pmatrix} L_X \\ L_Y \\ L_Z \end{pmatrix} \quad (3)$$

where  $H_0$  and  $\delta_0$  are the hour-angle and declination of the phase reference position, and  $\lambda$  is the wavelength corresponding to the center frequency of the receiving system. The elements in the transformation matrix in (Equation 3) are the direction cosines of the  $(u,v,w)$  axis relative to  $(X,Y,Z)$  axes. Thus as the interferometer observes a point source on the celestial sphere, the rotation of the Earth causes the  $u$  and  $v$  components of the baseline to trace out an elliptical locus. This ellipse is simply the projection onto the  $(u,v)$  plane of the circular locus traced out by the tip of the baseline vector, and at any instant the correlator output provides a measure of the visibility at two points in the  $(u,v)$  plane. For an East-West baseline  $L_Z=0$ , and a single ellipse is centered on the  $(u,v)$  origin.

The characteristics and specifications of CSRH-I are shown in Table.1. This array has 64 fre-

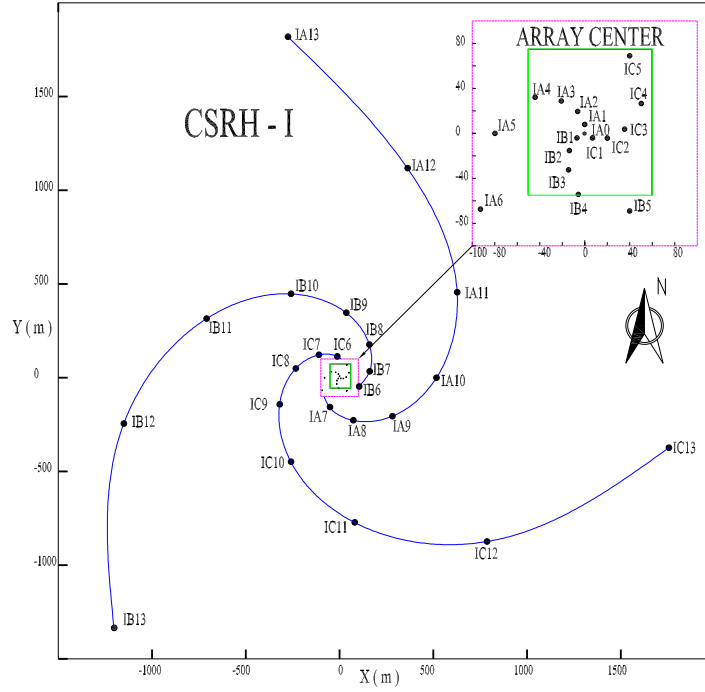


**Fig. 2** The 2D configuration of CSRH-I, the antennas are arranged in three spiral arms (named A axis, B axis and C axis respectively), every axis has 13 antennas, IA0 is in the center of the antenna array, its correspondent coordinate is (0,0)m, the locations of other antennas are reference to IA0 antenna, the black circle shown in this figure is the location of each antenna

**Table 1** CSRH-I characteristics and specifications

Observing band	0.4-2GHz
Spatial Resolution	51.6''-10.3''
Temporal Resolution	100 ms
Dynamic range of images	$\geq (25dB)$
Polarization	left and right circular polarization
frequency channel	64
Observing period	0UT to 8UT in winter, -1UT to 9UT in summer
antenna efficiency	$\geq (0.4)$
antenna noise temperature	$\leq (120K)$

introduced in further paper. To cover a wide frequency range with high sensitivity, the bandwidth of CSRH-I is divided into four sub bands: 0.4-0.8GHz, 0.8-1.2GHz, 1.2-1.6GHz and 1.6-2.0GHz. When the radio frequency (RF) signal of the Sun arrives at the analogue receiver of CSRH, it is mixed with two local oscillators. The first oscillator mixes the four sub bands at 3.6GHz, 4.0GHz, 4.4GHz and 4.8GHz respectively. So all the four sub bands become 2.8-3.2GHz after the operator of the first oscillator. Then, the output of the first oscillator is further mixed with the second oscillator at the frequency of 3.25GHz. Thus, the output frequencies of all the four sub bands range

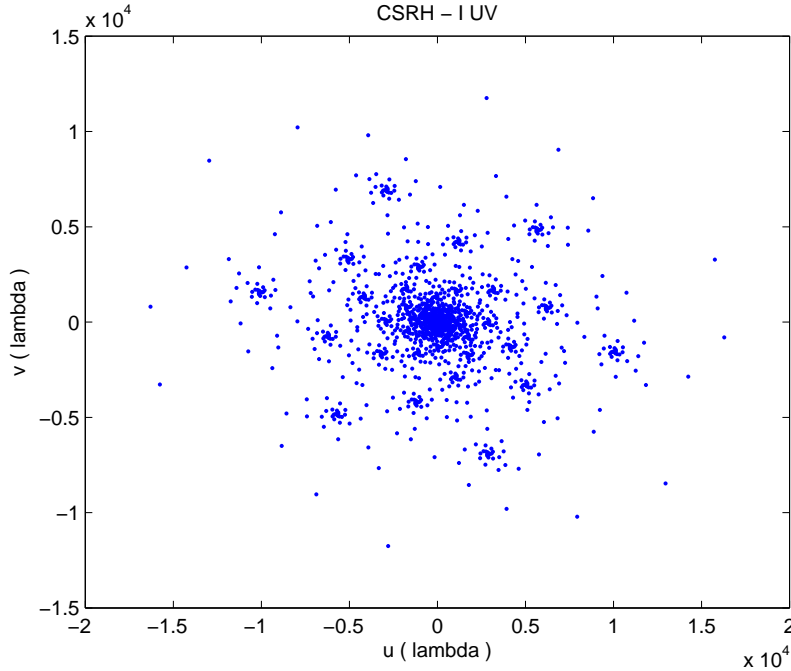


**Fig. 3**  $(u, v)$  coverage of CSRH-I. The blue points correspond to the locations of each  $(u, v)$  coverage of the source image. The number of the baselines is 780 for this radio heliograph. A stellar interferometer measures only one visibility per baseline.

In CSRH-I, to ensure all RF signals arriving simultaneously, the optic fibers transmitted the received RF signals of all channels with the same length. Each pair of two antennas is correlated to output a Fourier component of a solar radio image. Then we can reconstruct the brightness image through gathering all possible Fourier components from this interferometry.

## 2.2 Simulation of the radiation pattern for the feed and reflector antenna system

CSRH is an ultra wide band radio heliograph, in reference to choosing feed used in CSRH, there are many kinds of ultra wide band feeds (Taylor 1999) in antenna system but with some shortcomings. For example, ridged horn is too heavy and expensive; log-periodic antenna has variable phase center location and it spills over the edge of the dish to reduce the gain of the antenna system. In addition, the 3dB beamwidth of the radiation patterns of these two feeds are not wide enough, so the reflector surface cannot be fully illuminated by the feed, which will result in the low usage of the reflector antenna. For CSRH, we use Eleven feed to receive radio signals. Because it has many advantages, such as a fixed phase center location, well-shaped radiation patterns and low return loss. This feed is comprised of 13 folded dipoles. The bandwidth is decided by the ratio of the length of the "next-to-shortest" dipole to the length of the "next-to-longest" dipole. "next-to-shortest" means the shorter dipole of the two adjacent dipoles and "next-to-longest" means the longer dipole of the two adjacent dipoles. The length of the longest dipole is given by the wavelength of the lowest frequency. (Figure 4) gives the photo of CSRH-I feed. In the simulating stage, we

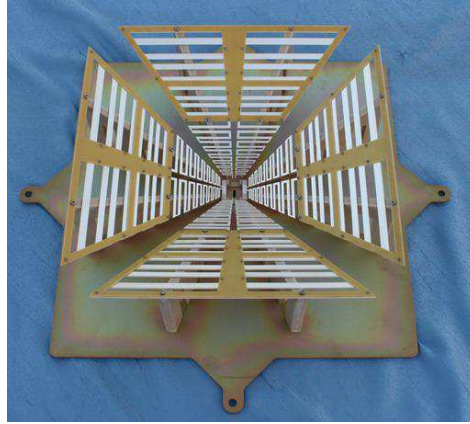


**Fig. 4** The photo of CSRH-I feed

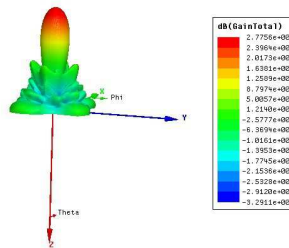


**Fig. 5** Simulated 3D radiation pattern of feed and reflector antenna in 0.4GHz, the right scale shows different colors corresponding to different values of Gain total in dB

feed and reflector antenna system of CSRH. In order to get good radiation pattern, dipoles in different heights vary one by one (Qing 1999) according to the optimized scaling ratio. Then, the derived radiation pattern of the feed is substituted to the feed and reflector antenna model, we can obtain the radiation pattern of the whole system. (Figure 5), (Figure 6) and (Figure 7) show the simulated 3D radiation patterns of the feed and reflector antenna system at 0.4GHz, 1.2GHz and 2GHz respectively. The feed is located in the focus of the parabolic reflector antenna, the pattern is symmetric about the z-axis. We can see that the radiation patterns behave a good symmetrical property on boresight.

To check the consistence between the simulated and measured radiation patterns, we observed Fengyun-2E satellite at 1.7GHz. This satellite bacon signal is received by IA0 antenna. The antenna moves in up and down directions and in left and right directions, so the measured radiation

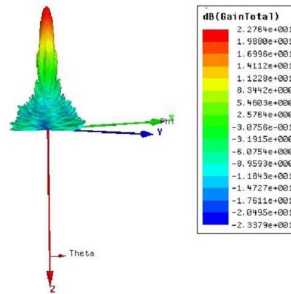


**Fig. 6** Simulated 3D radiation pattern of feed and reflector antenna in 1.2GHz, the right scale shows different colors corresponding to different values of directivity total in dB

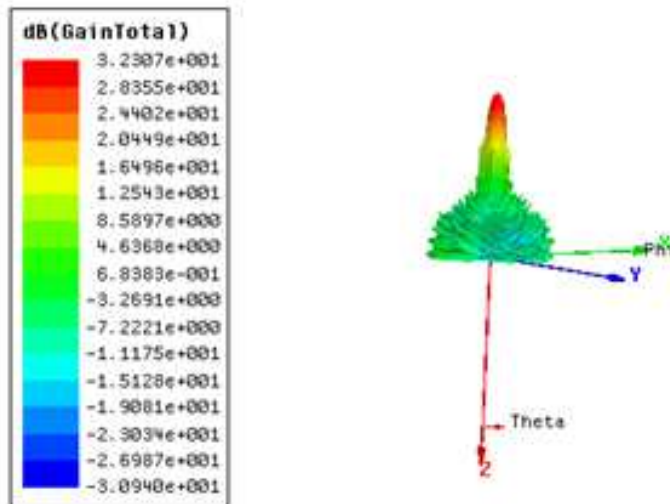


**Fig. 7** Simulated 3D radiation pattern of feed and reflector antenna in 2GHz, the left scale shows different colors corresponding to different values of Gain total in dB

maximum satellite downlink signal independently. The simulated and measured radiation patterns are illustrated at 1.7GHz in (Figure 8).

In antenna system, the parameter  $G$  is measured using two antennas (IB11 and IA0). IB11 was connected to a signal source, and it radiated signal to IA0, IA0 received signal from the source and the spectrum analyzer was connected with IA0. The ratio of the powers from the signal source and from the spectrum analyzer could be obtained, we could get the measured antenna gain  $G$  from (Equation 4).

$$G = \frac{P_{IA0}}{P_{IB11}} \quad (27000 \sim 31000) \quad (4)$$

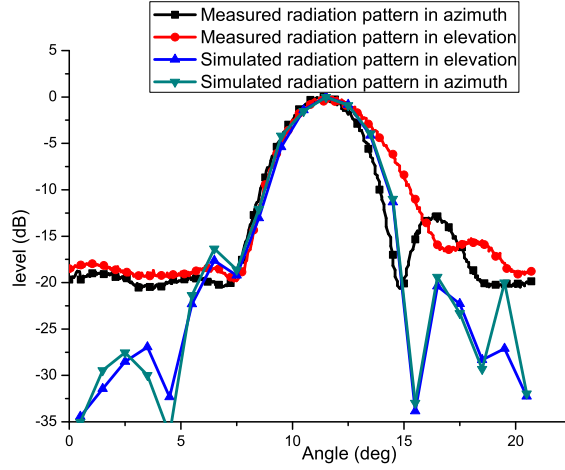


**Fig. 8** Simulated and measured 2D radiation pattern in 1.7GHz, the black line with square and red line with circle represent radiation pattern in elevation and azimuth directions; the blue line with up triangle and the dark cyan line with down triangle represent radiation pattern in elevation direction and azimuth directions

where  $\theta_{azimuth}$  and  $\theta_{elevation}$  are 3dB beamwidths in azimuth and elevation directions (Kildal 2009). The directivity coefficient  $D$  is calculated by (Equation 5).

$$D = \left( \frac{\pi d}{\lambda} \right)^2 \quad (5)$$

where  $d$  and  $\lambda$  represent the diameter of the reflector antenna and the wavelength of the working frequency. From (Equations 4) and (Equations 5), the measured  $G$  and calculated  $D$  are 34.61dB, 38.08dB respectively. Thus, the relationship between  $G$ ,  $D$  and antenna efficiency  $\eta$  is expressed in Equation 6):

$$G = D * \eta \quad (6)$$

then, we calculated  $\eta$  is 0.45, which is satisfied with the specification of the antenna design.

### 2.3 The equatorial mount and pointing error of the reflector antenna of CSRH

To facilitate the observation of the Sun, the reflector antenna of CSRH is designed with equatorial mount(also called polar mount) and use the quadrupod structure to support the feed, the foot points of this quadrupod are located at the edge of reflector antenna to reduce the influence of the plane wave incoming. The equatorial mount is a mount for instrument that follows the rotation of the sky (celestial sphere) by having one rotational axis parallel to the Earth's axis of rotation. In addition, it makes all the antennas operating consistently. The monitoring subsystem sends control signal to the operating unit of an antenna, and the antenna reacts the signal to adjust its posture working in the best condition.

The pointing error of each antenna is very important to an extended source such as the quiet Sun. If the pointing error of the antenna is not accurate, it would influence the phase correlation,

CSRH is less than 9'. When all the antennas point to the Sun after calibration, the response of the receivers must be uniform over the whole angular range of the observation.

### 3 ANTENNA NOISE TEMPERATURE

#### 3.1 Theoretical analysis of antenna noise temperature

In CSRH program, it is necessary to choose better amplifier (Kildal 2009) matching the antenna system. The antenna and receiver system noise temperature must be lower than the specification of the whole system.

The classical method of measuring antenna noise temperature is based on detection of astronomical source and sky background. These measurements could be extended for judging the system independent of the telescope antenna. Signals coming from the sky background noise and astronomical source need to be measured at frequencies supported by the antenna-feed. With the requirement of solar radio observation, the antenna noise temperature (Kildal 1995) is measured in the whole system. It relies on the reflector configuration and the feed radiation pattern, which means that if the feed has low sidelobe and cross polarization (Olsson 2006), the reflection from the ground plane will be reduced. At the same time, it could minimize the spillover from the sidelobes and the selection of feed is vital to the whole antenna system.

When observing solar radio signals, the circular polarization (Uralov 1998) is demonstrated from studies of large numbers of storms. The characteristic of the wave is effected by the terms of antenna gain, effective aperture, antenna noise temperature and so on. The reduction of the system noise temperature could improve the sensitivity of a radio telescope (Li 2015). Minimizing radio noise temperature usually involves cooling the amplifier from the front end of the system. It is convenient to use cosmic sources with small angular as a calibrated source, because the flux density of these sources is already known. Regarding the Sun, it is impossible to use a cosmic source because the Sun is stronger than any other sources. Thus, a noise source as a standard source is equipped in the input port of the analogue system. The input port is connected to the load, the antenna observation of sky background and the standard noise generator sequentially, the output data is gathered to compute antenna noise temperature. The thermal noise sources used in this measurement is resistor which is connected to receiver by coaxial lines. The noise temperature of the receiver and antenna system is measured by Y factor method. The factor Y is represented by:

$$Y = 10^{(P1-P2)/10} \quad (7)$$

where  $P1$  and  $P2$  correspond to the powers of different loads added in the end of the system. After obtaining Y, the antenna noise temperature  $T_A$  is computed by

$$T_A = (T_0 + T_r - Y \times T_r)/Y, \quad (8)$$

where  $T_0$  represents the ambient temperature,  $T_0 = 290K$ ,  $T_r$  means the temperature of the analogue receiver.

The noise temperature of the whole system is the antenna system noise temperature and re-

powers with different loads. In these equations,  $k = 1.3806505 \times 10^{(-23)}$  J/K,  $B$  represents the bandwidth,  $G_r$  is the gain of the system coming from the noise source of the receiving system. the noise temperature  $T_{NS}$  means terminal connecting with the noise source,  $T_{50} = 290K$ , the noise temperature  $T_{50}$  means terminal connecting with standard impedance  $50\Omega$ ,

$$[(T_{50} + T_r) kB] + [G_r] = [P_{50}] \quad (9)$$

$$[(T_{NS} + T_r) kB] + [G_r] = [P_{NS}] \quad (10)$$

$$[(T_A + T_r) kB] + [G_r] = [P_{SKY}] \quad (11)$$

The square brackets in (Equation 9), (Equation 10), (Equation 11) mean that the unit of each value is dB. From (Equation 12), (Equation 13), (Equation 14), we could get the representations of  $T_r$ ,  $G_r$  and  $T_A$  respectively.

$$T_r = \frac{T_{NS} - T_{50} \left( \frac{P_{NS}}{P_{50}} \right)}{\frac{P_{NS}}{P_{50}} - 1} \quad (12)$$

$$G_r = \frac{P_{50} \left( \frac{P_{NS}}{P_{50}} - 1 \right)}{kB (T_{NS} - T_{50})} \quad (13)$$

$$T_A = \frac{P_{sky}}{P_{50}} (T_{50} + T_r) - T_r \quad (14)$$

### 3.2 The measured results of CSRH

For CSRH radio heliograph, we test the gain by using Y factor method (Penzias 1965) in the whole system. (Table 2) gives the measured noise temperatures of the noise source at different frequencies. The relationship between Excess Noise Ratio(ENR) and the noise source temperature is:

$$ENR = \frac{T_{NS} - T_0}{T_0} \quad (15)$$

Where,  $T_0$  is the ambient temperature,  $T_0 = 290K$ . From (Table 2), it can be observed that the noise temperature decreases as the frequency increases. (Table 3) lists the noise powers of different terminals: noise source,  $50\Omega$  impedance, sky background and the Sun. Based on the measured results of (Table 3), we can calculate system noise ( $T_r$ ), system Gain ( $G_r$ ) and antenna noise temperature ( $T_A$ ) by using (Equation 12), (Equation 13), and (Equation 14) respectively. The calculated results are shown in (Table 4). The fourth column of this table gives the measured antenna noise temperature, they all less than the specification 120K in different frequencies.

## 4 DATA PROCESSING FOR CSRH-I

### 4.1 Solar radio burst observation

A solar radio burst instance is provided to validate the effectiveness of CSRH, this event occurred on November 12, 2010. By using a 5-element system of CSRH-I, we successfully observed a solar radio burst with an associated X-ray flare C1.5 class. In Huairou observatory station, SBRS also observed this instance at the same time. Another instrument called GOES also observed this event

**Table 2** The noise temperatures ( $T_{NS}$ ) of the noise source at different frequencies, ENR means the multiple number of the noise source above the ambient temperature, this value could be tested according to an instrument.

Radio frequency(GHz)	ENR(dB)	Noise temperature(K)
0.75	21.28	392230.18
0.8	21.03	37051.90
1.025	20.57	33357.24
1.2	20.18	30517.21
1.45	19.82	28112.62
1.95	18.71	21837.56

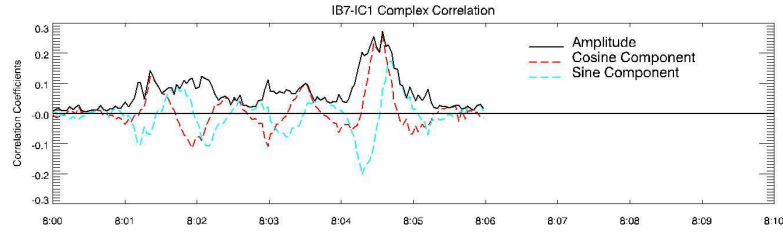
**Table 3** The noise powers of the different terminals including noise generator,  $50\Omega$  impedance, sky background and the Sun at different frequencies ( $P_{NS}$ ,  $P_{50}$ ,  $P_{sky}$ , and  $P_{sun}$  represents the measured powers of the terminals.)

Radio frequency(GHz)	$P_{NS}$ (dBm)	$P_{50}$ (dBm)	$P_{sky}$ (dBm)	$P_{sun}$ (dBm)
0.75	-26.19	-44.93	-46.58	-39.25
0.8	-24.98	-42.81	-44.42	-37.83
1.025	-22.21	-40.52	-42.78	-35.65
1.2	-28.31	-44.6	-46.36	-41.5
1.45	-29.81	-46.80	-48.57	-42.13
1.95	-28.86	-43.61	-45.2	-41.5

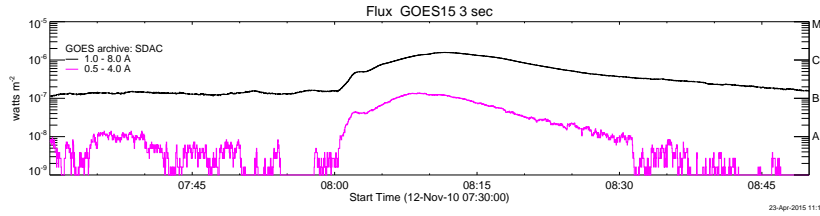
**Table 4** The measured system noise ( $T_r$ ), system Gain ( $G_r$ ) and antenna noise temperature ( $T_A$ ) at different frequencies

Radio frequency(GHz)	$T_r(K)$	$G_r(dB)$	$T_A(K)$
0.75	268.3	61.7	92.9
0.8	326.05	63.12	99
1.025	235.7	66.4	58.9
1.2	437.3	60.61	48
1.45	308.3	59.9	69.8
1.95	456.42	61.49	61.17

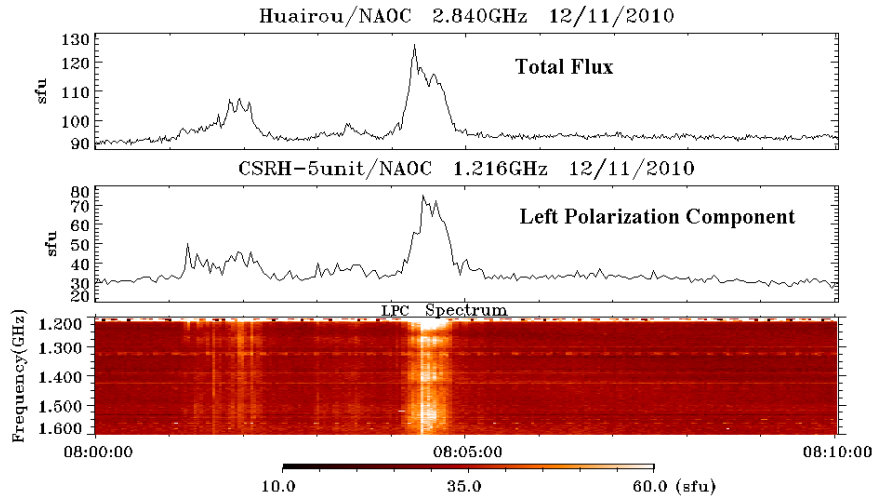
IC1 are two antennas of CSRH-I, the black curve shows the amplitude of the fourier component, the red and blue curves show cosine and sin components; (Figure 9) (b) gives the flux density of GOES at wavelength of 1-8 Angstrom showing in black line and 0.5-4 Angstrom drawing in red line; (Figure 9) (c) shows the total flux density of Huairou instrument observation and IC1



(a) Observed fringe included the sin and cosine components



(b) The flux density observed by GOES



(c) The measured result obtained by IC1

**Fig. 9** The comparison between different instruments observations

#### 4.2 Satellite image using Aperture synthesis method

In reference to CSRH-I image calibration, the diameter of the antenna is too small to use non-solar compact sources as calibrating sources. Therefore, we use Fengyun-2E satellite source as a point source in the beginning stage of CSRH establishment at 1.7GHz. The observed result of Fengyun-2E is drawn in (Figure 10), there are totally 930 fourier components using 31 antennas, each pair of these antennas is interfered to provide a fourier component of the observed source. The brightness image of the observed source can be obtained (Wang 2013) through applying inverse fourier transform to the gathered fourier components.

For detecting satellite source, observation is obtained during the pass of the source through a stationary beam. (Figure 10) shows the Stokes parameter I, which represents the total intensity of the satellite source. The phase error of spherical waves coming from satellite source would be

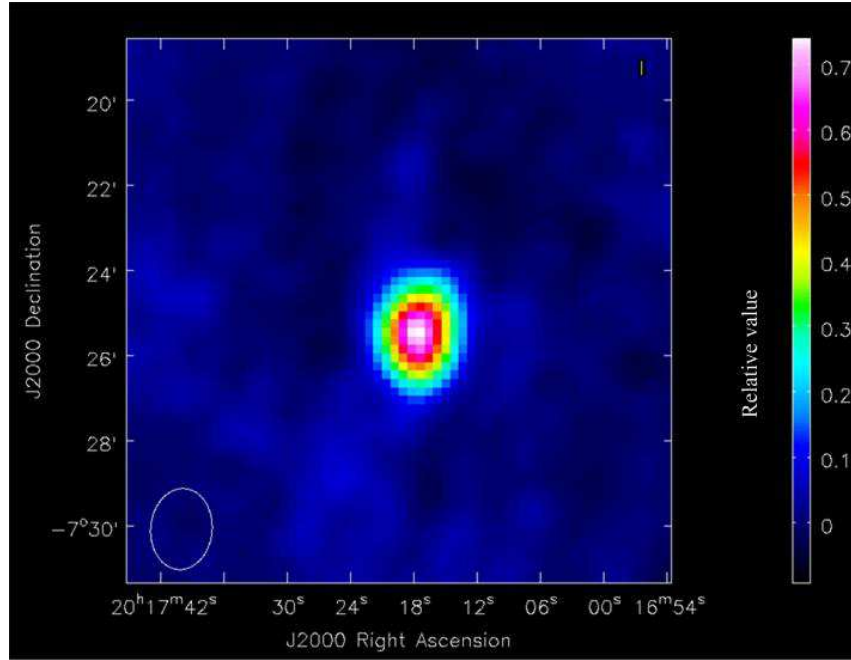


**Fig. 10** Stokes parameter I: the cleaned observed image of Fengyun-2E satellite at 1.7GHz on June 4th, 2013, the ellipse in the lower left corner is the synthesized beam, the vertical scale bar represents the relative level of the background

error could be removed successfully using two observations. (Figure 10) is obtained from CASA, the integration time is 30ms and the beam size of this image corresponding to the antenna beam is  $1.25^{\circ} \times 2.489^{\circ}$ . This observation shows the good performance of the imaging capability of CSRH-I.

## 5 CONCLUSION

The characteristics of CSRH are presented in this paper. From these data, we could know that the system gain  $G_r$  is larger than 60dBi and antenna noise temperature  $T_A$  is less than 120K respectively, which are satisfied with the specifications of our science requirement. After some of the antennas installed in Mingantu Observatory, a solar radio burst at 1.302GHz was successfully captured by CSRH 5-element on 2010, November 12, at the same time, SBRS and GOES also observed this event. Another result is about the point source of satellite image at 1.7GHz, which shows the imaging ability of this system. CSRH will establish solar radio images in decimeter and centimeter wavelength more accurately.

**Acknowledgements** We acknowledge the anonymous referee for his/her valuable suggestions and comments of this paper. The author also wish to thank Long Xu, Chong Huang, Cheng Ming Tan, Jing Huang, for their lots of advice on this paper. This work is supported by NSFC grants (Nos.: MOST2011CB81140111221063, 10778605, 11003028, 11203042, U1231205), National Major Scientific Equipment Research and Design project (ZDYZ2009-3).

## References

- Bastian T.S., Benz, A.O., Gary, D.E., 1998, ARA&A, 36, 131
- Chen J.J., Bai Z.R., Luo A.L., Zhao Y.H., 2014, RAA, 15, 607
- Penzias A. A., Wilson, R. W., 1965, The Astronomical Journal, 142, 1149
- Aghdam K. M. P., Farajj-Dana R., Rashed-Mohassel J., 2005, IEEE Proc. Microw. Antennas Propag., 59,392
- Liu Z., Gary D. E., Nita G. M., White S. M., Hurford G. J., 2007, Publications of the Astronomical Society of the Pacific, 119, 307
- Uralov A. M., Grechnev V. V., Lesovoi S. V., Sych R. A., Kardapolova N. N., Smolkov G. Ya, Treskov T. A., 1998, Solar Physics, 178, 119
- Kildal P. S., 2009, Chalmers University, Chalmers, 44
- Kildal P. S., Sipus, Z., 1995, IEEE Proc. Microw. Antennas Propag., 37,114
- Nakajima H., Nishio M., Enome S., 1994, IEEE Proc. Microw. Antennas Propag., 82,705
- Olsson R., Kildal P. S., Weinreb S., 2006, IEEE Proc. Microw. Antennas Propag., 54,368
- Qing X. M., Chia Y. W. M. 1999, Electron. Lett., 35,2154
- Yan Y., Zhang J., Wang W., Liu F., Chen Z., Ji G., 2008, Earth, Moon, and Planets, 104,1
- Sergey V. Lesovoi, Alexander T. Altyntsev, Eugene F. Ivanov, Alexey V. Gubin, 2014, RAA, 864
- Wang W., Yan Y. H., Liu D. H., Chen Z. J., Su C., Liu F., Geng L. H., Chen L. J., Du J., 2013, PASJ, 65, sp18-1
- Li S., Yan Y. H., Chen Z. J., Wang W., Zhang F.S., 2015, PASA, 32, 1
- Taylor G. B., Carilli C. L., Perley R. A., 1999, ASP Conf. Ser. v. 11
- Lindsay D. Mi, Howell C, K., 2008, The Journal of the Astronautical Sciences, 56,71
-